ELSEVIER

Materials Science and Engineering A 418 (2006) 146–154

MATERIALS SCIENCE & ENGINEERING A

www.elsevier.com/locate/msea

Fatigue damage and fracture behavior of tungsten fiber reinforced Zr-based metallic glassy composite

H. Zhang, Z.F. Zhang *, Z.G. Wang, K.Q. Qiu, H.F. Zhang, Q.S. Zang, Z.Q. Hu

Shenyang National Laboratory for Materials Science, Institute of Metal Research, Chinese Academy of Sciences, 72 Wenhua Road, Shenyang 110016, PR China

Received in revised form 10 November 2005; accepted 21 November 2005

Abstract

The fatigue life, damage and fracture behavior of tungsten fiber reinforced metallic glass $Zr_{41.25}Ti_{13.75}Ni_{10}Cu_{12.5}Be_{22.5}$ composites are investigated under cyclic push–pull loading. It is found that the fatigue life of the composite increases with increasing the volume fraction of tungsten fibers. Similar to crystalline metals, the regions of crack initiation, propagation and overload fracture can be discerned on the fracture surface of the specimen. Fatigue crack normally initiates in the metallic glass matrix at the outer surface of the composite specimen and propagates predominantly in the matrix. Different crack front profile around the tungsten fibers and fiber pullout demonstrate that fatigue crack may propagate around the fiber, leading to bridging of the crack faces by the unbroken fiber and hence improved fatigue crack-growth resistance. Locally decreased effective stiffness in the region where fiber distribution is sparse may provide preferential crack path in the composite. A proposed model was exercised to elucidate different tungsten fiber fracture morphologies in the fatigue crack propagation and overload fracture regions in the light of Poisson's ratio effect during fatigue loading.
© 2005 Published by Elsevier B.V.

Keywords: Metallic glass; Composite; Tungsten fiber; Cyclic loading; Fatigue crack

1. Introduction

Recent years, bulk metallic glasses have gained continued research in many aspects including processing of multi-component alloys with high glass-forming ability and investigations of their mechanical properties [1–4]. They have been considered as advanced materials for future engineering applications because of their interesting mechanical properties which are different from those for crystalline alloys in many aspects, such as high static and dynamic strength, lower elastic modulus and high Charpy impact fracture energy [5,6]. Fracture mechanisms of metallic glasses under tensile and compressive loads have been explained by considering the combined effect of normal and shear stress on the fracture processes [7,8]. Although bulk metallic glasses exhibit no macroscopic plastic deformation at ambient temperature in tensile and compressive tests, their fracture toughness and fatigue behavior are similar to those of crystalline metals and alloys [9–17]. The measured fracture toughness of Zr-based metallic glasses was in the range of 18–84 MPa $m^{1/2}$ using fatigue precracked specimens [18–21]. Such fracture toughness values are much higher than that of the coarser-grained, crack-bridging toughened ceramics [22]. In addition, the high fatigue strength of bulk metallic glasses is related to their surprisingly high static strength. From the stress/life tests (S–N curves), the fatigue limit of the bulk metallic glasses when defined by the ratio of fatigue strength to ultimate fracture strength is in the range of 4–30% [10,23]. This may be caused by different fatigue mechanisms as well as by a lack of microstructural barriers to fatigue cracks of amorphous alloys compared to conventional metals and alloys. Some fatigue studies have established that bulk metallic glasses were susceptible to fatigue degradation, which results in a fatigue exponent m of 1–2 in the Paris power law relationship [16,17,20,24].

Among the multi-component Zr-based bulk metallic glasses, $Zr_{41.25}Ti_{13.75}Cu_{12.5}Ni_{10}Be_{22.5}$ has been investigated widely because of its excellent glass-forming ability and superior mechanical properties [4,25]. Bulk metallic glasses were observed to fail along narrow shear bands in tensile or compres-

* Corresponding author. Tel.: +86 24 2397 1043; fax: +86 24 2389 1320.
E-mail address: zhfzhang@imr.ac.cn (Z.F. Zhang).

0921-5093/$ – see front matter © 2005 Published by Elsevier B.V.
doi:10.1016/j.msea.2005.11.038

sive tests at ambient temperature without macroscopic plastic elongation [7,8]. Therefore, many efforts have been devoted to improve the plasticity of bulk metallic glasses. A bulk metallic glass composite containing ductile dendrites synthesized through an in situ processing method exhibited remarkable compressive and tensile plasticity due to the interaction between ductile dendrites and shear bands [26–28]. High compressive plasticity was also observed in some particle reinforced metallic glass composites [29]. It is proposed that the reinforcements may restrict the propagation of shear bands, prompting the formation of multiple shear bands.

The tungsten fiber reinforced metallic glass composite has been observed to fail along a single adiabatic shear band at high strain rates and show self-sharpening behavior during ballistic impact. This behavior makes it have some potential applications, such as kinetic energy penetrator [30]. Substantially improved plasticity in metallic glass composites has also been found in metallic glass matrix composites reinforced with continuous tungsten and steel fibers [30–33]. Conner et al. [31] performed compression and tension experiments on tungsten or steel fiber reinforced $Zr_{41.25}Ti_{13.75}Cu_{12.5}Ni_{10}Be_{22.5}$ metallic glass composites with different fiber volume fraction (V_f). Multiple shear bands were observed in the metallic glass matrix under compression, leading to a large increase in compressive plasticity as well as a high fracture strength. Under tension, the largest increase in strength and strain to failure was obtained in the 60% V_f steel wire reinforced composite having weakly bonded fiber/matrix interface. Mode II cracking at the fiber/matrix interface and fiber pullout may contribute to the enhanced toughness of the composite [31].

Although fiber reinforced metallic glass composites exhibit promising fracture strength and certain plasticity, their deformation and fracture behavior under cyclic loading have received little attention. In order to use metallic glass composite as engineering material, their fatigue behavior is a major concern. The main goal of the present article is to examine the failure mechanisms influencing deformation behavior and fatigue in a tungsten fiber reinforced metallic glass composite, with particular emphasis on the role of fibers in delaying crack growth, and therefore enhancing toughness of the composite.

2. Materials and experimental procedure

The materials studied in the present investigation are a unidirectional tungsten fiber reinforced bulk metallic glass composites with glassy matrix of $Zr_{41.25}Ti_{13.75}Ni_{10}Cu_{12.5}Be_{22.5}$. The composites were synthesized by induction melting method using high purity metals under argon atmosphere. Tungsten fibers with diameter of around 300 μm were straightened and cleaned in acetone using ultrasonic cleaning followed by ethanol cleaning. Ingots of the matrix material were melted in a resistive furnace and infiltrated into the reinforcement. The quartz tube filled with reinforcement and matrix was then quenched in a brine solution. Complete details of the processing methods are described elsewhere [32,33].

Tungsten fiber distribution in the metallic glass $Zr_{41.2}Ti_{13.8}Cu_{12.5}Ni_{10}Be_{22.5}$ composite is typified by the back scatter SEM micrograph, as shown in Fig. 1a. To reveal the detailed microstructure in the metallic glass matrix, a back scatter SEM micrograph with higher magnification is shown in Fig. 1b. Similar to some other tungsten fiber composite, the tungsten/matrix interface reactant is rare [33]. Plate-like and polygonal crystalline phases are present in the glassy matrix. Energy dispersive X-ray spectroscopy (EDX) analysis revealed that the plate-like phase is a Zr-rich phase, while the polygonal phase is a Be-rich phase.

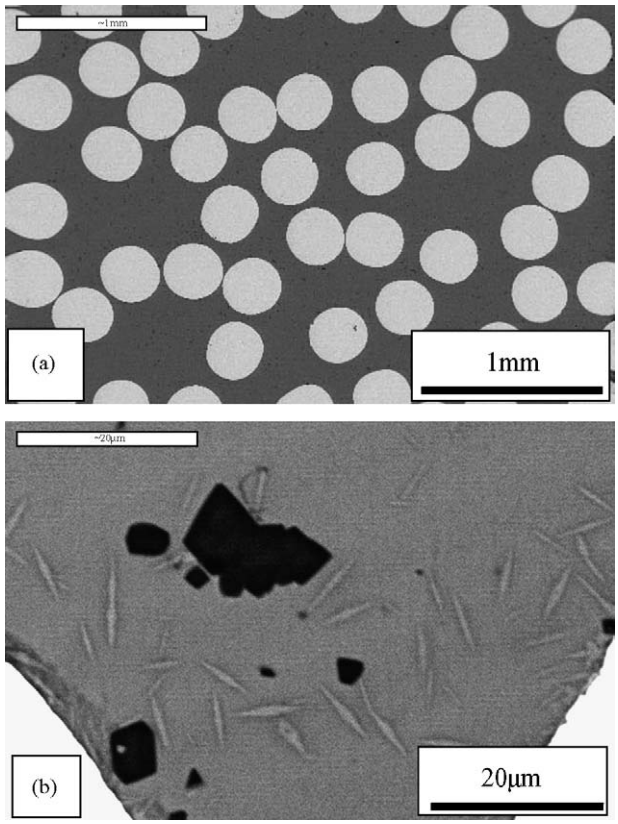

Fig. 1. Back scatter scanning electron micrographs showing (a) distribution of tungsten fibers in the metallic glass $Zr_{41.2}Ti_{13.8}Cu_{12.5}Ni_{10}Be_{22.5}$ composite and (b) crystalline phases in the glassy matrix.

The fatigue specimens were cut by wire electrical discharge machining to have a 10 mm long gauge with rectangular cross-section. Tungsten fibers in the specimens were arranged in the direction parallel to the loading axis. Before fatigue tests, all the specimens were mechanically polished for surface observation. Cyclic push–pull load was applied to the specimens under constant load control and the strain was measured by an extensometer attached on one side of the specimen. Fatigue lifetimes were measured at a selected stress amplitude of 550 MPa. Fatigue tests were run at a frequency of 1 Hz (sinusoidal waveform) and a load ratio of $R = -1$ using a MTS 10 KN servo-hydraulic testing machine at room temperature in air. Tungsten fiber volume fractions in the three composite specimens are 18, 26 and 37%, respectively, which were determined by calculating the area that fibers occupy on the fracture surface, as shown in Section 3.2. Fatigue tests were terminated when the specimens fractured and the number of cycles to failure was defined as fatigue life. All the fractured specimens were investigated by a Cambridge S360

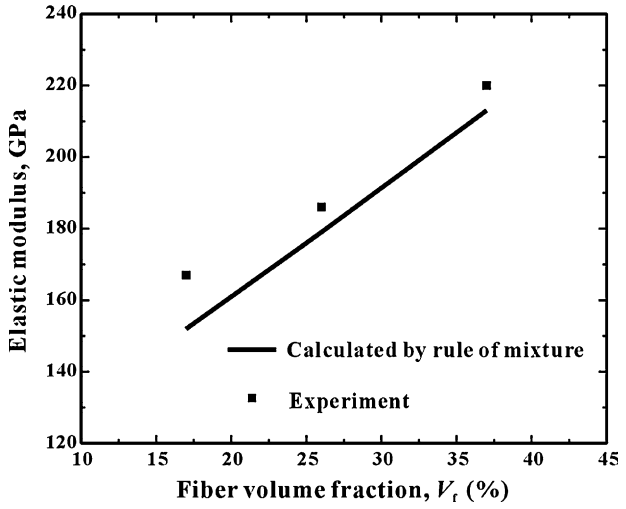

Fig. 2. Plot of the elastic moduli of tungsten fiber reinforced metallic glass $Zr_{41.2}Ti_{13.8}Cu_{12.5}Ni_{10}Be_{22.5}$ composite as a function of fiber volume fraction. The straight line is the elastic modulus calculated by the rule of mixture.

scanning electron microscopy (SEM) to reveal the deformation morphology and fracture features.

3. Results and discussion

3.1. Fatigue life of the composites

Tungsten fiber and metallic glass matrix are in their elastic range at the selected stress amplitude of 550 MPa. The variation of elastic modulus, which is defined as the slope of the stress–strain curves in the tensile part of the first cycle, with fiber volume fraction is shown in Fig. 2. It is noted that elastic modulus of the composite increases with increasing fiber volume fraction. As shown in Fig. 2, the calculated elastic modulus E_c based on the rule of mixtures is as below:

$$E_c = E_m(1 - V_f) + E_f V_f \quad (1)$$

Here subscripts c, m and f represent composite, matrix and fiber, respectively. E_m and E_f have been obtained elsewhere [16,31]. It is apparent that the measured elastic modulus is comparable to that calculated by the rule of mixtures.

Fig. 3a shows cyclic strain response of the tungsten fiber reinforced metallic glass composites with different fiber volume fractions at a push–pull stress amplitude of 550 MPa. For comparison, the cyclic strain and fatigue lifetime of the fully amorphous and partially crystallized alloy $Zr_{41.2}Ti_{13.8}Cu_{12.5}Ni_{10}Be_{22.5}$ are also shown in the figure [16]. Fatigue life of the composite increases with increasing fiber volume fraction, indicating that fatigue life can be increased by adding the tungsten fibers (Fig. 3b). Cyclic strain amplitudes for the composites are much lower than that for the unreinforced metallic glass at the same cyclic stress amplitude. Besides, strain amplitude tends to decrease when the fiber volume fraction changes from 18 to 37%, reflecting a good stiffening effect of the tungsten fibers. It can be seen from Fig. 3a that, for all the amorphous alloys and composites, the cyclic strain amplitude nearly maintains constant, i.e. no cyclic hardening or softening occurred. This is consistent with the lack of work hardening ability in fully bulk metallic glasses [7,13,15].

3.2. Fractography observations

Fracture surface for the 18% V_f tungsten fiber/$Zr_{41.25}Ti_{13.75}Ni_{10}Cu_{12.5}Be_{22.5}$ composite is shown in Fig. 4a. Such fracture surface morphology is strongly suggestive of fatigue failure in ductile metals and alloys. Crack initiated from the surface flaw of the glassy matrix, as indicated by the arrow in Fig. 4a. Obvious fiber/matrix interface debonding was observed at a tungsten fiber close to the crack initiation site, as shown in Fig. 4a. Copious microcracks were observed within the fiber, whereas no obvious microcrack can be observed within the fibers far away from the crack initiation site in this figure.

To further discern crack initiation and growth regions as well as microcrack distribution within tungsten fibers, a back scatter micrograph is presented in Fig. 4b. The regions of crack initiation, stable crack propagation and overload fracture can be clearly seen. Fatigue crack normally initiated from the surface flaw in the glassy matrix because no tungsten fiber is seen near

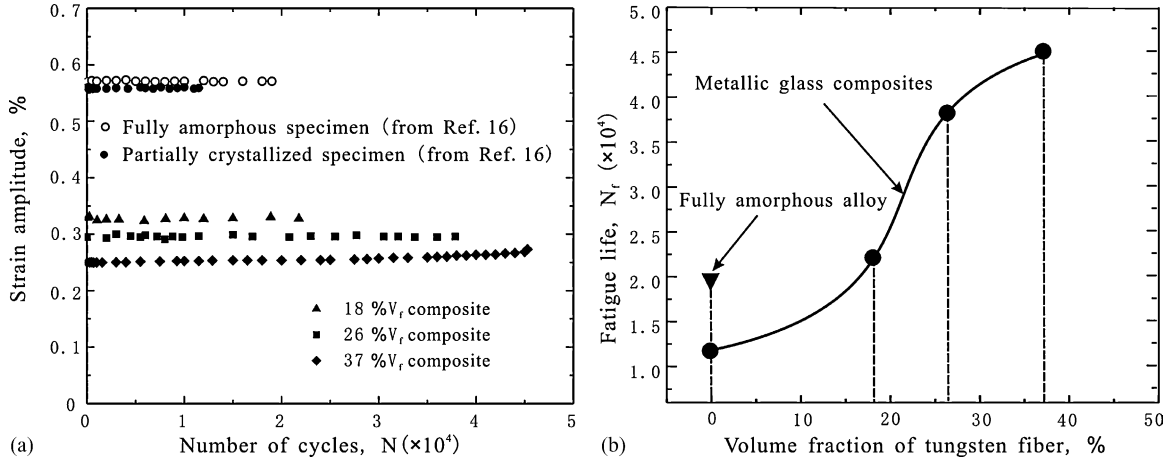

Fig. 3. (a) Cyclic strain response curves of three tungsten fiber reinforced metallic glass $Zr_{41.2}Ti_{13.8}Cu_{12.5}Ni_{10}Be_{22.5}$ composites and two unreinforced bulk metallic glasses at a stress amplitude of 550 MPa and (b) relation of fatigue life vs. volume fraction of tungsten fibers in the composites.

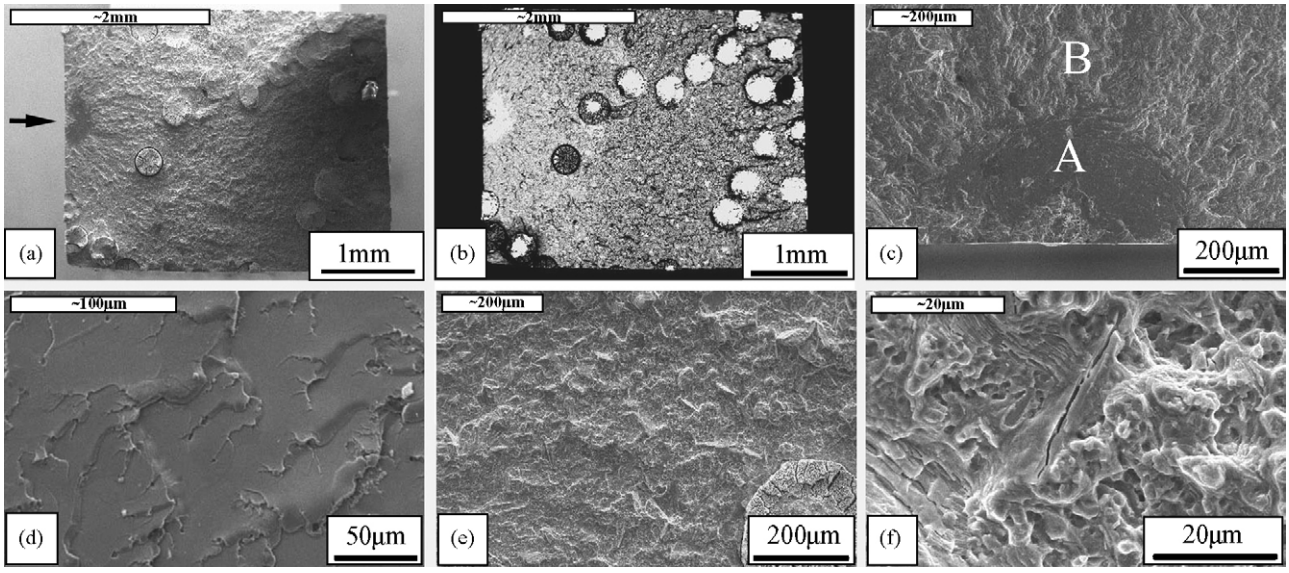

Fig. 4. Scanning electron micrographs of the fractures surface for the composite with 18 vol% tungsten fiber. Macroscopic fatigue fractography observed by SEM (a) and back scatter image (b); (c) fatigue crack initiated from a surface flaw of the glass matrix; (d) relatively flat region adjacent to crack initiation site; (e) fatigue crack propagation region; (f) higher magnification image of region B in 'c', showing a local cracking in the crystalline phase.

that site. After initiation of the crack, it propagated inwards into a relative flat region (marked by 'A') and then into a region with radiating characterization (marked by 'B'), as shown in Fig. 4c. Region A consists of a microscopically smooth area separated by curved steps, as shown in Fig. 4d. Substantially enhanced surface roughness compared to region A was observed in region B (Fig. 4e) which represents steady fatigue crack propagation stage of the composite. High magnification micrograph of crack propagation region B is shown in Fig. 4f. The fracture surface is quite irregular and composed of ductile microvoids and periodic markings. Crack can be seen in the plate-shaped phase, showing brittle nature of the crystalline phase.

In order to further understand the role of fibers in retarding fatigue crack propagation, fracture surface at different regions of the composite was investigated in more detail. Fig. 5a shows three tungsten fibers (with different deformation morphology) near the fatigue crack initiation site on the fracture surface of the composite. Copious microcracks are visible on the two fibers (A and B) closer to the crack initiation site. There are more microcracks in fiber A which is closer to crack initiation site than fiber B, as shown in the figure. Besides, fiber/matrix debonding in fiber A was observed (Fig. 5b). These microcracks in fiber A are clearly seen on higher magnification micrograph in Fig. 5c. Even though microcracks were also observed in fiber B, there is a lack of microcracks in the central part of the fiber, as clearly seen in Fig. 5d.

Microcracks can only be observed locally in tungsten fibers near fiber/matrix interface on the overload fracture surface of the composite (Fig. 6a and b), and their amount is less than that in fibers A and B in the fatigue region. The local microcracks are clearly seen on the higher magnification micrographs in Fig. 6c and d. Based on microcrack distribution on fiber fracture surfaces in the crack propagation and overload regions, it is deduced that microcracks formed easily in the fatigue region and that its amount increases when fatigue crack tip approached and passed through the fibers. Therefore, the fiber, closest to the crack initiation site, damages seriously.

Fig. 7 shows the SEM micrograph of the overload fracture region for the glassy matrix. No evidence of vein-like morphology caused by viscous flow typical of fully amorphous alloys is observed. The fracture surface is characterized by cleavage crack in the plate-like crystalline phases and ductile microvoids. The formation of these microvoids may originate from the brittle polygonal crystalline phases. As part of elastic energy has been released during fatigue crack propagation and formation of microcracks around polygonal and plate-like crystalline phases, no adiabatic shear band will form in the overload fracture region.

Fig. 8a and b show back scatter SEM micrographs of the fracture surfaces in the composite containing 26 and 37% V_f tungsten fiber, respectively. Even though it is difficult to locate precisely the crack initiation sites in the two specimens, it can be observed that crack initiated from the surface flaw of glassy matrix which was located at the bottom side and bottom-right corner of the specimen with 26 and 37% V_f fibers, respectively, as shown in Fig. 8a and b. This fatigue region A exhibits lighter color compared to overload region B in these back scatter micrographs. White dotted curves are drawn to separate the fatigue region from the overload region, as shown in Fig. 8a and b. It can be seen that the fracture surface roughness in the fatigue region is lower than that in the overload region, consistent with the observation that fracture surface toughness scaled with local crack growth rates in bulk amorphous alloys [20]. Based on this partition, the region of crack initiation and propagation covers about one-third of the fracture surface. This proportion is much higher than that in the unreinforced fully amorphous alloys [16]. Unlike unreinforced amorphous alloys, the fatigue crack front propagated quite unevenly through the composites, with the fatigue crack propagating predominantly in the glassy matrix and round the fibers. For the three composites studied here, fatigue cracks were always seen to initiate and propagate in the area with few

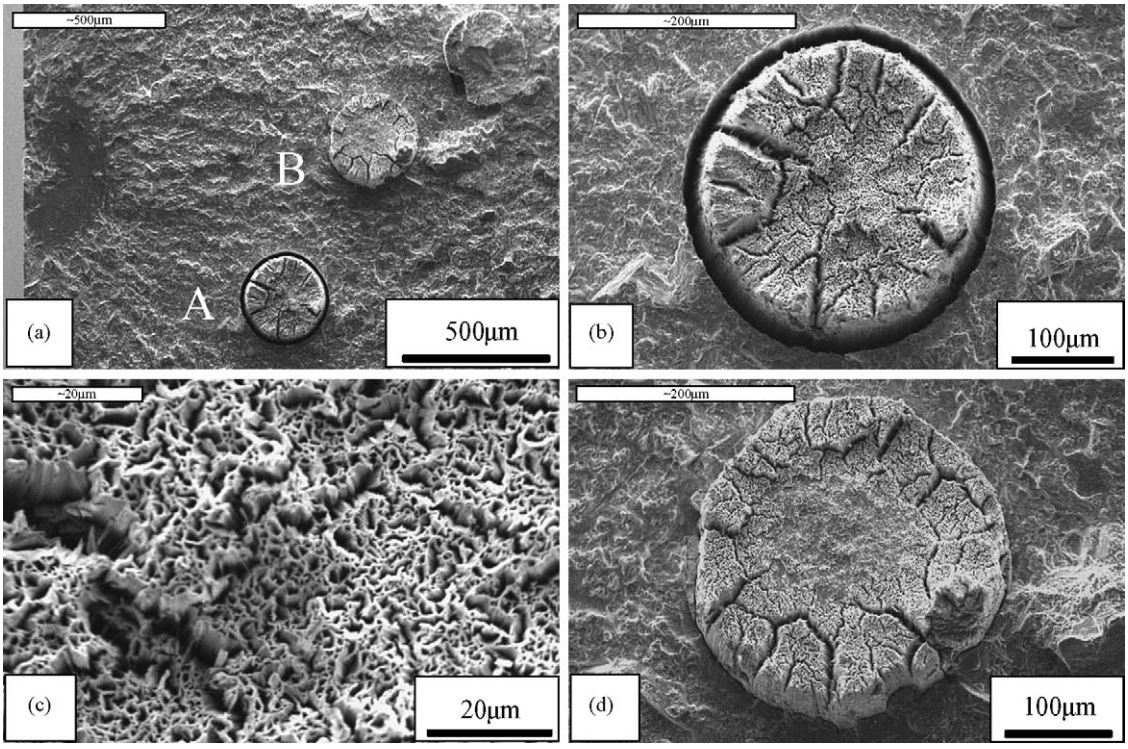

Fig. 5. Scanning electron micrographs showing deformation morphologies of tungsten fiber in the fatigue crack propagation region. (a) Low magnification of two fibers marked by A and B; (b) fracture morphology of tungsten fiber A closest to the crack initiation site. The fiber is full of copious microcracks; (c) higher magnification image of fiber A showing copious microcracks; (d) fracture morphology of tungsten fiber B. No microcracks can be seen in the central part.

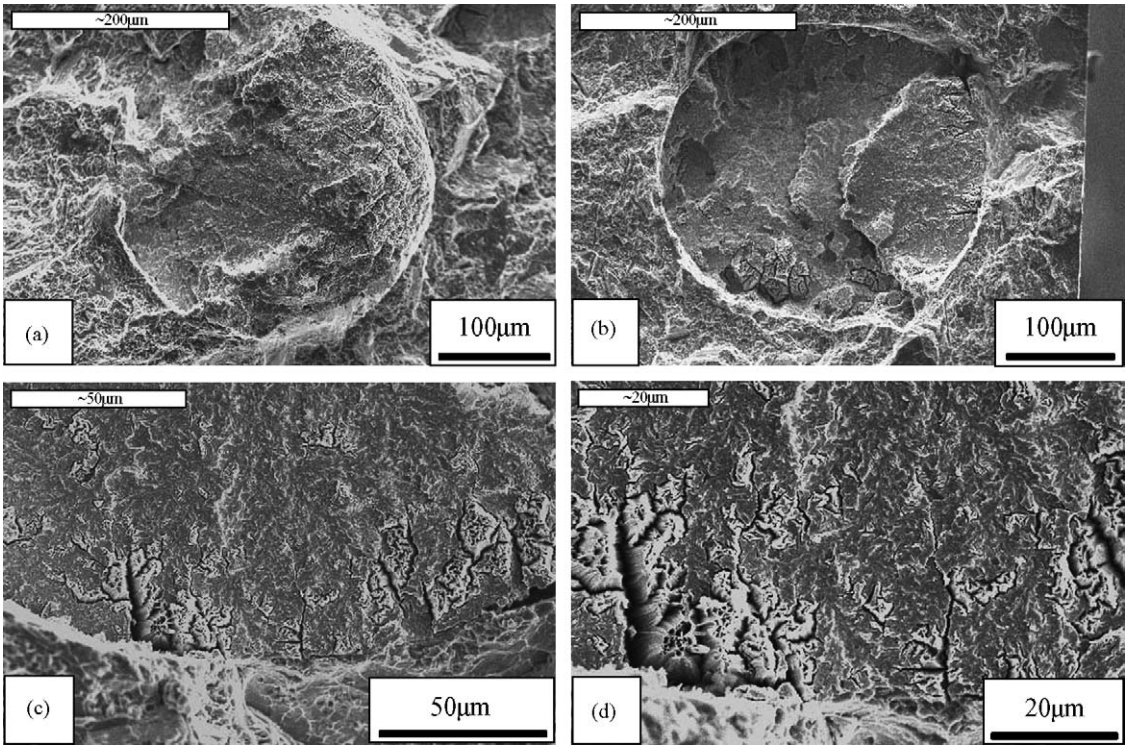

Fig. 6. Fracture morphologies of the tungsten fibers in the overload region of the composite observed at low magnification (a) and (b), and high magnification (c) and (d). Local microcracks can only be seen near the fiber/matrix interface.

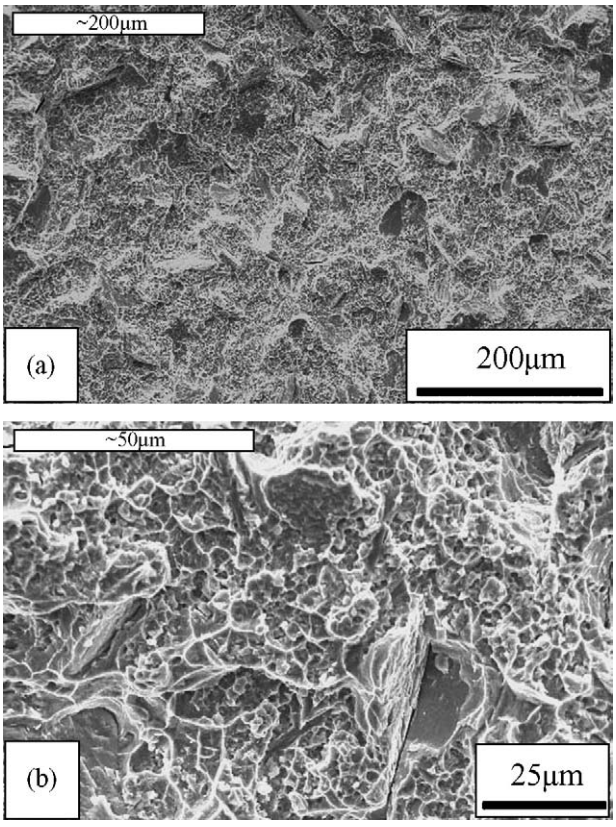

Fig. 7. Scanning electron micrographs of metallic glass matrix in the overload fracture region observed at low magnification (a) and high magnification (b).

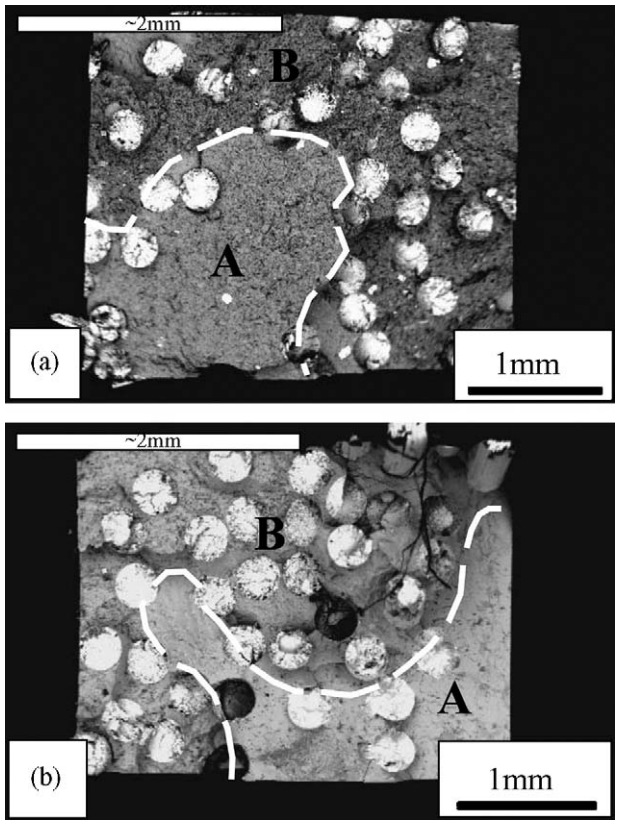

Fig. 8. Scanning electron micrographs of the fracture surfaces in the composites with fiber volume fraction of: (a) 26 vol% and (b) 37 vol%. White dotted curves represent the boundaries between fatigue crack propagation and overload fracture regions.

tungsten fibers. This indicates that the tungsten fibers play an important role in retarding crack propagation, which is consistent with the enhanced fatigue life in the composite containing high volume fraction of tungsten fibers.

Deformation and fracture of the tungsten composites are mainly confined to a narrow region near fracture surface, whereas no crack was observed on the other position of the specimen surfaces. Normally the composites exhibit flat fracture surface with few fiber pullout, as shown in Fig. 9a. Fiber/matrix interface morphology can be observed from higher magnification micrograph of specimen surface in the tungsten composite in Fig. 9b. No obvious debonding can be discerned, reflecting strong fiber/matrix bonding.

3.3. Crack growth path in the tungsten fibers/$Zr_{41.25}Ti_{13.75}Cu_{12.5}Ni_{10}Be_{22.5}$ composite

For the three tungsten fibers/$Zr_{41.25}Ti_{13.75}Cu_{12.5}Ni_{10}Be_{22.5}$ composites, their fatigue lives are longer than that of the unreinforced metallic glasses. From the fracture surfaces, the effect of tungsten fibers in retarding crack growth is prominent based on the following observations. First, the area of fatigue crack initiation and stable propagation for the composites is much larger than that of the unreinforced BMG [16]. Secondly, the crack path is substantially changed when encountering fibers, passing predominantly through the area with sparse fiber distribution. This means that fatigue cracks will change its path when encountering fibers and propagate predominantly through the matrix. A typical example of the crack path on the fracture surface can be seen in Fig. 8a and b. This phenomenon can be easily understood by considering the effect of tungsten fiber volume fraction. Suppose that there exist two regions with different fiber volume fractions in the front of a fatigue crack in the tungsten fibers/$Zr_{41.25}Ti_{13.75}Cu_{12.5}Ni_{10}Be_{22.5}$ composite, as schematically illustrated in Fig. 10. The preferential crack path in the two regions can be calculated based on stiffness and strain of the composite. Suppose fiber volume fraction in region B (V_f^B) is higher than that in region A (V_f^A), i.e. $V_f^B > V_f^A$. Based on the rule of mixtures, the elastic moduli of the composite in regions A and B, E_c^A and E_c^B, are calculated as:

$$E_c^A = E_m(1 - V_f^A) + E_f V_f^A \quad (2a)$$

$$E_c^B = E_m(1 - V_f^B) + E_f V_f^B, \quad (2b)$$

where E_m and E_f are elastic moduli of matrix and fiber. When the composite is subjected to a load parallel to the fiber direction, region B will have a higher elastic modulus (and therefore higher stiffness) than region A, i.e. $E_c^B > E_c^A$. Correspondingly, the local strain in region B should be lower than that in region A because of locally increased effective stiffness of the composite in region B. Therefore, the crack opening displacement (COD) in the matrix of region B will be lower than that in region A at the same tensile stress level during cyclic loading. In addition, the nearer the crack tip approaches the fiber, the greater the apparent

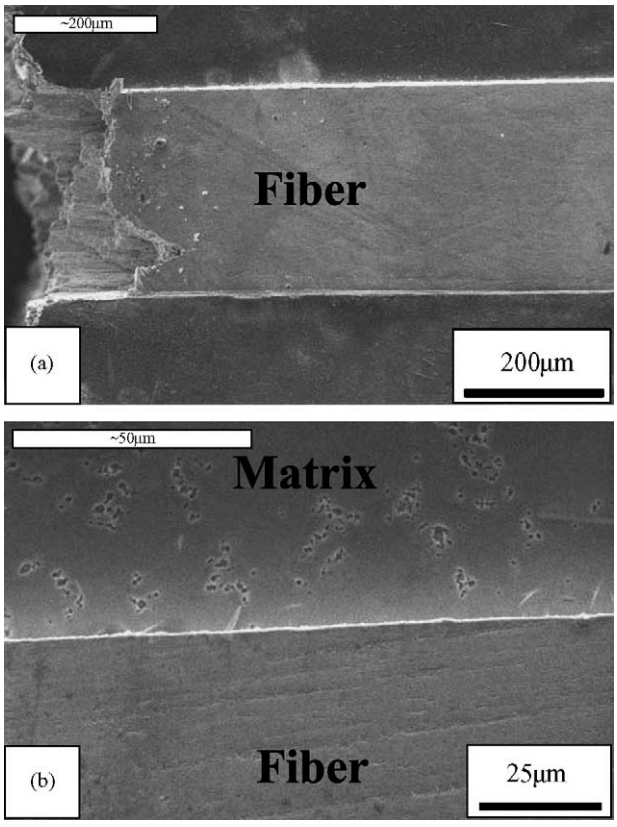

Fig. 9. Scanning electron micrographs of specimen surfaces in tungsten fiber reinforced metallic glass composite after fatigue loading. (a) Relatively flat fracture surface and short distance of fiber pullout resulting from strong interfacial bonding and (b) higher magnification of specimen surface showing well-bonded tungsten/matrix interface without interfacial microcracks.

stiffness in the matrix is. This is due to a strong bonding between the fiber and the matrix [34]. All these suggest that fatigue crack will preferentially propagate in the region without fibers or with few fiber distributions.

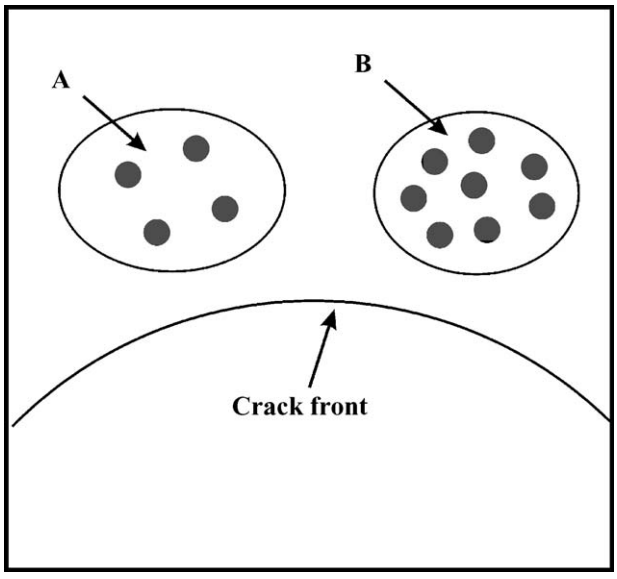

Fig. 10. Schematic illustration of tungsten fiber distribution in two different regions A and B in front of the fatigue crack.

3.4. Microcrack formation mechanisms within tungsten fibers

Copious microcracks were observed on fracture surfaces of tungsten fibers which were located in the fatigue crack growth region. However, microcracks were only observed locally on fracture surfaces of the fibers in the overload region. For all the tungsten fibers on the fracture surface of composite, it was observed that cracks always formed along radial direction and serious damage of fibers frequently occurred near the fiber/matrix interfaces (Fig. 5b and d). The formation of these microcracks can be explained based on the difference in the Poisson's ratio between the glassy matrix and tungsten fiber in the composite. As the coefficiency of thermal expansion (CTE) of tungsten fiber is lower than that of the metallic glassy matrix, triaxial residual stress exists in both fiber and matrix for the tungsten fiber composites. In tungsten fibers, both axial and transverse stresses are compressive. In the metallic glassy matrix, while both axial and tangential stresses are tensile, the radial stress is compressive [31].

When the tensile load is applied in the axial direction, Poisson effect of fiber and matrix may cause transverse contraction of the composite. The transverse strain in matrix and fiber, ε_m^t and

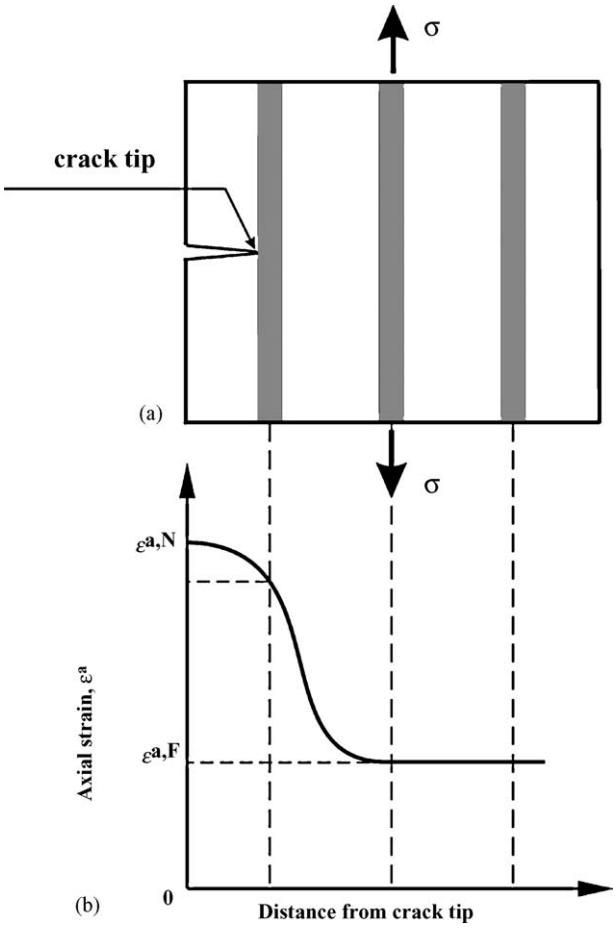

Fig. 11. Schematic illustration of (a) crack tip sketch relative to fiber and matrix in the composite and (b) axial strain distribution in the glassy matrix as a function of distance from the crack tip.

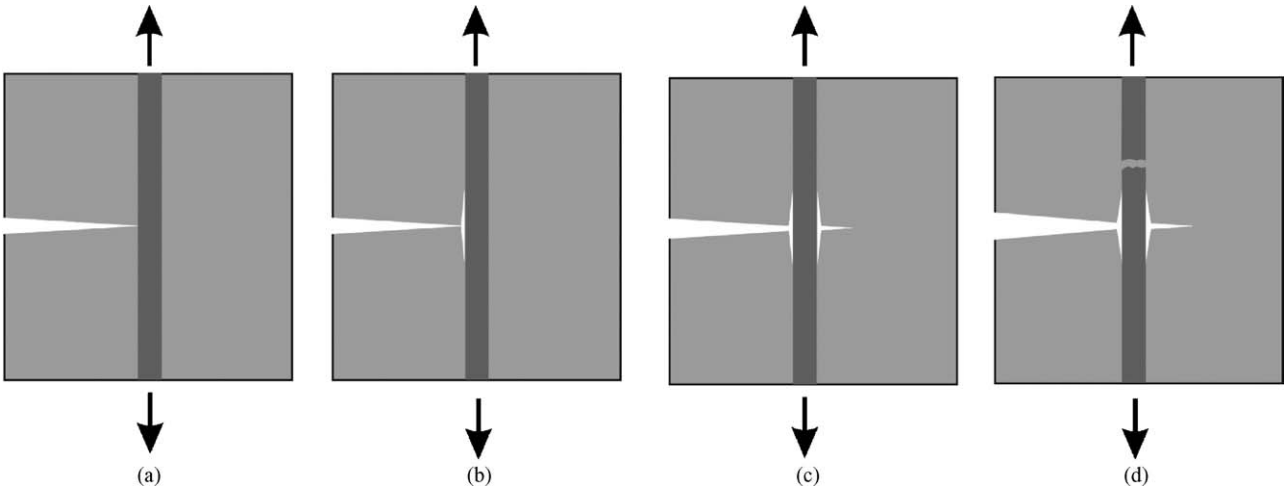

Fig. 12. Schematic illustration of toughening mechanisms by fiber in the tungsten fiber reinforced metallic glass matrix composite under fatigue loading.

ε_f^t, are defined as:

$$\varepsilon_m^t = \varepsilon_m^a \times \nu_m \,(\text{matrix}) \tag{3a}$$

$$\varepsilon_f^t = \varepsilon_f^a \times \nu_f \,(\text{fiber}) \tag{3b}$$

where subscripts m and f represent matrix and fiber, respectively. ε_m^a and ε_f^a represent axial strains in the matrix and the fiber. ν_m and ν_f are Poisson's ratios of the matrix and the fiber and are equal to 0.36 and 0.28, respectively [31]. During the tensile half cycle, fiber and matrix may have the same axial strain, i.e. $\varepsilon^a = \varepsilon_m^a = \varepsilon_f^a$, because of a strong interfacial bonding between the fiber and the matrix, as seen in Fig. 9b. From Eqs. (3a) and (3b), we can obtain differential transverse strain $\Delta\varepsilon^t$ between the matrix and the fiber:

$$\Delta\varepsilon^t = \varepsilon_m^t - \varepsilon_f^t = \varepsilon^a(\nu_m - \nu_f). \tag{4}$$

The difference $(\nu_m - \nu_f)$ in the Poisson's ratio should be constant in the whole specimen. However, due to high stress concentration near the crack tip the average axial strain near the crack tip, $\varepsilon^{a,N}$, must be obviously higher than the strain far away from the crack tip, $\varepsilon^{a,F}$, i.e.

$$|\varepsilon^{a,N}| \gg |\varepsilon^{a,F}|. \tag{5}$$

The value ε^a depends on the distance to fatigue crack tip. This can be schematically illustrated in Fig. 11a and b. From Eqs. (4) and (5), we deduce that the differential transverse strain near the crack $|\Delta\varepsilon^{t,N}|$ must be higher than that far away from the crack tip, $|\varepsilon^{t,F}|$, i.e.

$$|\Delta\varepsilon^{t,N}| \gg |\Delta\varepsilon^{t,F}|. \tag{6}$$

The higher differential transverse strain near the crack tip, $|\Delta\varepsilon^{t,N}|$, will lead to a higher transverse stress at the fiber and the matrix. Therefore, from Eq. (6), the transverse stress near the crack tip, $\sigma^{t,N}$, must be substantially higher than that far away from the crack tip, $\sigma^{t,F}$, i.e.

$$|\sigma^{t,N}| \gg |\sigma^{t,F}|. \tag{7}$$

From Eq. (7), it can be concluded that the cyclic stresses on the two positions (near and far away from the crack tip) differ significantly. Therefore, during cyclic loading, there exists transverse fatigue loading on fibers both near to and far away from the fatigue crack tip. Microcracks will initiate and propagate easily within the fibers near the fatigue crack tip at higher transverse stress amplitude during tension-compression cyclic loading (Fig. 4b) and even occupy the whole tungsten fiber (Fig. 5b). On the other hand, microcracks are difficult to initiate inside the tungsten fibers far away from the fatigue crack tip (Fig. 6a and b) because the transverse stress amplitude applied to the tungsten fiber is relatively low. Occasionally, a few microcracks were observed at periphery of the tungsten fiber in the overload region of the composite (Fig. 6c and d).

Based on observations on fracture morphologies of the tungsten composite, the toughening mechanisms of the tungsten fibers in the composite can be schematically illustrated in Fig. 12. As the fatigue crack propagates into the fiber/matrix interfacial region under cyclic loading (Fig. 12a), tensile stress concentration and shear stress along interface will cause tungsten fiber/matrix interfacial debonding (Fig. 12b). Part of the energy is absorbed by both the newly formed interface and microcracks inside the fibers (Fig. 5), which will result in a reduced fatigue crack-growth rate. When subjected to further cyclic loading, fatigue crack will propagate around the tungsten fiber, with a resultant debonding of the whole interface near the fatigue crack face (Fig. 12c). The fiber may not fracture at this time when the fatigue crack propagates beyond the fiber, leading to a bridging effect by the unbroken fiber. This bridging traction will screen the matrix crack tip from the applied far field load, leading to a decrease in the effective stress intensity experienced at the crack tip. When subjected to further cyclic loading, the fiber may fracture at a weak spot away from the crack face, and the fatigue crack will further propagate in the matrix (Fig. 12d). As the fatigue cycles increase, the matrix may still grip the broken fiber through frictional force at the fiber/matrix interface before pullout of the fiber from the matrix, further increasing the toughness of the composite.

4. Conclusions

Fatigue life of the tungsten fibers/$Zr_{41.25}Ti_{13.75}Cu_{12.5}Ni_{10}Be_{22.5}$ metallic glass composites is longer than that of the unreinforced metallic glasses. For the three composites investigated, the specimen with higher fiber volume fraction exhibits superior fatigue crack growth resistance and higher fatigue life. Fatigue cracks initiated from the surface flaw of the glassy matrix and propagated predominantly in the matrix under the applied stress amplitude. Crack will be retarded when encountering tungsten fibers and will propagate round the fibers, leading to a bridging effect by the unbroken fiber. Interfacial debonding, copious mirocracks within the fibers and bridging effect may cause the enhanced toughness of the tungsten fibers/$Zr_{41.25}Ti_{13.75}Cu_{12.5}Ni_{10}Be_{22.5}$ composites.

Acknowledgements

We thank G. Yao, J.L. Wen, H.H. Su and W. Gao for technical assistance and stimulating discussions. This work was supported by the National Natural Science Funds of China (NSFC) under grant No. 50401019 and the “Hundred of Talent Project” by the Chinese Academy of Sciences.

References

[1] W.L. Johnson, in: W.L. Johnson, A. Inoue, C.T. Liu (Eds.), Bulk Metallic Glasses, Materials Research Society, Warrendale, PA, 1999, pp. 311–339.
[2] A. Inoue, Acta Mater. 48 (2000) 279–306.
[3] A. Inoue, T. Zhang, T. Masumoto, Mater. Trans. JIM 30 (1989) 965–972.
[4] A. Peker, W.L. Johnson, Appl. Phys. Lett. 63 (1993) 2342–2344.
[5] W.L. Johnson, Bulk Glass-Forming Metallic Alloys: Science and Technology, MRS Bulletin, Materials Research Society, Pittsburgh, PA, October 1999, pp. 42–56.
[6] A. Inoue, Bulk Amorphous Alloys, Trans. Tech. Publications, 1998.
[7] Z.F. Zhang, J. Eckert, L. Schultz, Acta Mater. 51 (2003) 1167–1179.
[8] Z.F. Zhang, G. He, J. Eckert, L. Schultz, Phys. Rev. Lett. 91 (2003) 045505.
[9] C.J. Gilbert, R.O. Ritchie, W.L. Johnson, Appl. Phys. Lett. 71 (1997) 476–478.
[10] C.J. Gilbert, J.M. Lippmann, R.O. Ritchie, Scripta Mater. 38 (1998) 537–542.
[11] Z.F. Zhang, J. Eckert, L. Schultz, Metall. Mater. Trans. A 35 (2004) 3489–3498.
[12] Z.F. Zhang, J. Eckert, L. Schultz, J. Mater. Res. 18 (2003) 456–465.
[13] J.J. Lewandowski, Mater. Trans. 42 (2001) 633–637.
[14] K. Fujita, A. Inoue, T. Zhang, Mater. Trans. JIM 41 (2000) 1448–1453.
[15] P. Lowhaphandu, L.A. Ludrosky, S.L. Montgomery, J.J. Lewandowski, Intermetallics 8 (2000) 487–492.
[16] H. Zhang, Z.G. Wang, K.Q. Qiu, Q.S. Zang, H.F. Zhang, Mater. Sci. Eng. A356 (2003) 173–180.
[17] K.M. Flores, W.L. Johnson, R.H. Dauskardt, Scripta Mater. 49 (2003) 1181–1187.
[18] J.H. Schneibel, J.A. Horton, P.R. Munroe, Metall. Mater. Trans. A 32 (2001) 2819–2825.
[19] P. Lowhaphandu, J.J. Lewandowski, Scripta Mater. 38 (1998) 1811–1817.
[20] C.J. Gilbert, V. Schroeder, R.O. Ritchie, Metall. Mater. Trans. A 30 (1999) 1739–1753.
[21] J. Schroers, W.L. Johnson, Phys. Rev. Lett. 93 (2004) 255506.
[22] P.F. Becher, J. Am. Ceram. Soc. 74 (1991) 255–269.
[23] Y. Yokoyama, N. Nishiyama, K. Kukaura, H. Sunada, A. Inoue, Mater. Trans. JIM 40 (1999) 696–699.
[24] P.A. Hess, R.H. Dauskardt, Acta Mater. 52 (2004) 3525–3533.
[25] H.A. Bruck, T. Christman, A.J. Rosakis, W.L. Johnson, Scripta Mater. 30 (1994) 429–434.
[26] F. Szuecs, C.P. Kim, W.L. Johnson, Acta Mater. 49 (2001) 1507–1513.
[27] C.C. Hays, C.P. Kim, W.L. Johnson, Phys. Rev. Lett. (20002901-2904) 84.
[28] J. Das, M.B. Tang, K.B. Kim, R. Theissmann, F. Baier, W.H. Wang, J. Eckert, Phys. Rev. Lett. 94 (2005) 205501.
[29] R.D. Conner, H. Choi-Yim, W.L. Johnson, J. Mater. Res. 14 (1999) 3292–3297.
[30] H. Choi-Yim, R.D. Conner, F. Szuecs, W.L. Johnson, Scripta Mater. 45 (2001) 1039–1045.
[31] R.D. Conner, R.B. Dandliker, W.L. Johnson, Acta Mater. 46 (1998) 6089–6102.
[32] K.Q. Qiu, A.M. Wang, H.F. Zhang, B.Z. Ding, Z.Q. Hu, Intermetallics 10 (2002) 1283–1288.
[33] R.B. Dandliker, R.D. Conner, W.L. Johnson, J. Mater. Res. 13 (1998) 2896–2901.
[34] B. Harris, Metal Sci. 14 (1980) 351–362.